JOURNAL OF GEOPHYSICAL RESEARCH, VOL. 113, B05303, doi:10.1029/2007JB005211, 2008

Waveform modeling of historical seismograms of the 1930 Irpinia earthquake provides insight on "blind" faulting in Southern Apennines (Italy)

N. A. Pino,[1] B. Palombo,[2] G. Ventura,[3] B. Perniola,[4] and G. Ferrari[5]

Received 7 June 2007; revised 27 September 2007; accepted 22 January 2008; published 6 May 2008.

[1] The Southern Apennines chain is related to the west-dipping subduction of the Apulian lithosphere. The strongest seismic events mostly occurred in correspondence of the chain axis along normal NW–SE striking faults parallel to the chain axis. These structures are related to mantle wedge upwelling beneath the chain. In the foreland, faulting develops along E–W strike-slip to oblique-slip faults related to the roll-back of the foreland. Similarly to other historical events in Southern Apennines, the I_0 = XI (MCS intensity scale) 23 July 1930 earthquake occurred between the chain axis and the thrust front without surface faulting. This event produced more than 1400 casualties and extensive damage elongated approximately E-W. The analysis of the historical waveforms provides the chance to study the fault geometry of this "anomalous" event and allow us to clarify its geodynamic significance. Our results indicate that the M_S = 6.6 1930 event nucleated at 14.6 ± 3.06 km depth and ruptured a north dipping, N100°E striking plane with an oblique motion. The fault propagated along the fault strike 32 km to the east at about 2 km/s. The eastern fault tip is located in proximity of the Vulture volcano. The 1930 hypocenter, similarly to the 1990 (M_W = 5.8) Southern Apennines event, is within the Mesozoic carbonates of the Apulian foredeep and the rupture developed along a "blind" fault. The 1930 fault kinematics significantly differs from that typical of large Southern Apennines earthquakes, which occur in a distinct seismotectonic domain on late Pleistocene to Holocene outcropping faults. These results stress the role played by pre-existing, "blind" faults in the Apennines subduction setting.

Citation: Pino, N. A., B. Palombo, G. Ventura, B. Perniola, and G. Ferrari (2008), Waveform modeling of historical seismograms of the 1930 Irpinia earthquake provides insight on "blind" faulting in Southern Apennines (Italy), *J. Geophys. Res.*, *113*, B05303, doi:10.1029/2007JB005211.

1. Introduction

[2] In the Tyrrhenian Sea back-arc - Apennines chain subduction system (Italy) seismicity mainly occurs in the crust of the overriding plate at depth less than 15 km (Figure 1a) [*Chiarabba et al.*, 2005]. The events are related to the upward and lateral pushing of the Tyrrhenian mantle wedge above the subducting plate [*Ventura et al.*, 2007, and references therein]. In the NW-SE striking Southern Apennines belt, where the strongest earthquakes of Apennines occurred, the epicenters concentrate along the chain axis. Available focal mechanisms suggest prevailing normal faulting along NW-SE striking structures [*Frepoli and Amato*, 2000]. Moderate magnitude ($M_W \leq 6$) strike-slip events locate east of the chain axis (Figure 1b) [*Di Luccio et al.*, 2005a, 2005b]. In Southern Apennines, highly destructive earthquakes, e.g., the 1456, 1688, 1857, 1930, and 1980 events ($X \leq I_0 \leq XI$ MCS; Figure 1b), caused thousands of fatalities and only few of these had surface faulting [*Valensise and Pantosti*, 2001a; *DISS Woking Group*, 2006]. In this area, the seismic potential is high: the recurrence time of events with $M \geq 6.5$ is between 60 and 140 years [*Jenny et al.*, 2006].

[3] The Irpinia 1930 earthquake (M_e = 6.7) [*Gasperini et al.*, 1999] produced more than 1400 casualties and no surface faulting. On the basis of intensity [*Gasperini et al.*, 1999] and bulletin data [*Kárnik*, 1969], the epicenter is located between the chain axis and the foreland, about 15 km east of the main seismogenic belt defined by both historical and instrumental earthquakes (Figures 1b and 2). The damage area is approximately elongated in E-W direction [*Gasperini et al.*, 1999]. In the picture of the Southern Apennines seismotectonic setting, the location and the elongation direction of the damage area are relatively

[1] Istituto Nazionale di Geofisica e Vulcanologia, Osservatorio Vesuviano, Naples, Italy.
[2] Istituto Nazionale di Geofisica e Vulcanologia, Centro Nazionale Terremoti, Rome, Italy.
[3] Istituto Nazionale di Geofisica e Vulcanologia, Sismologia e Tettonofisica, Rome, Italy.
[4] Istituto di Fisica, Università degli Studi di Urbino, Urbino, Italy.
[5] SGA srl, Bologna, Italy.

0148-0227/08/2007JB005211$09.00

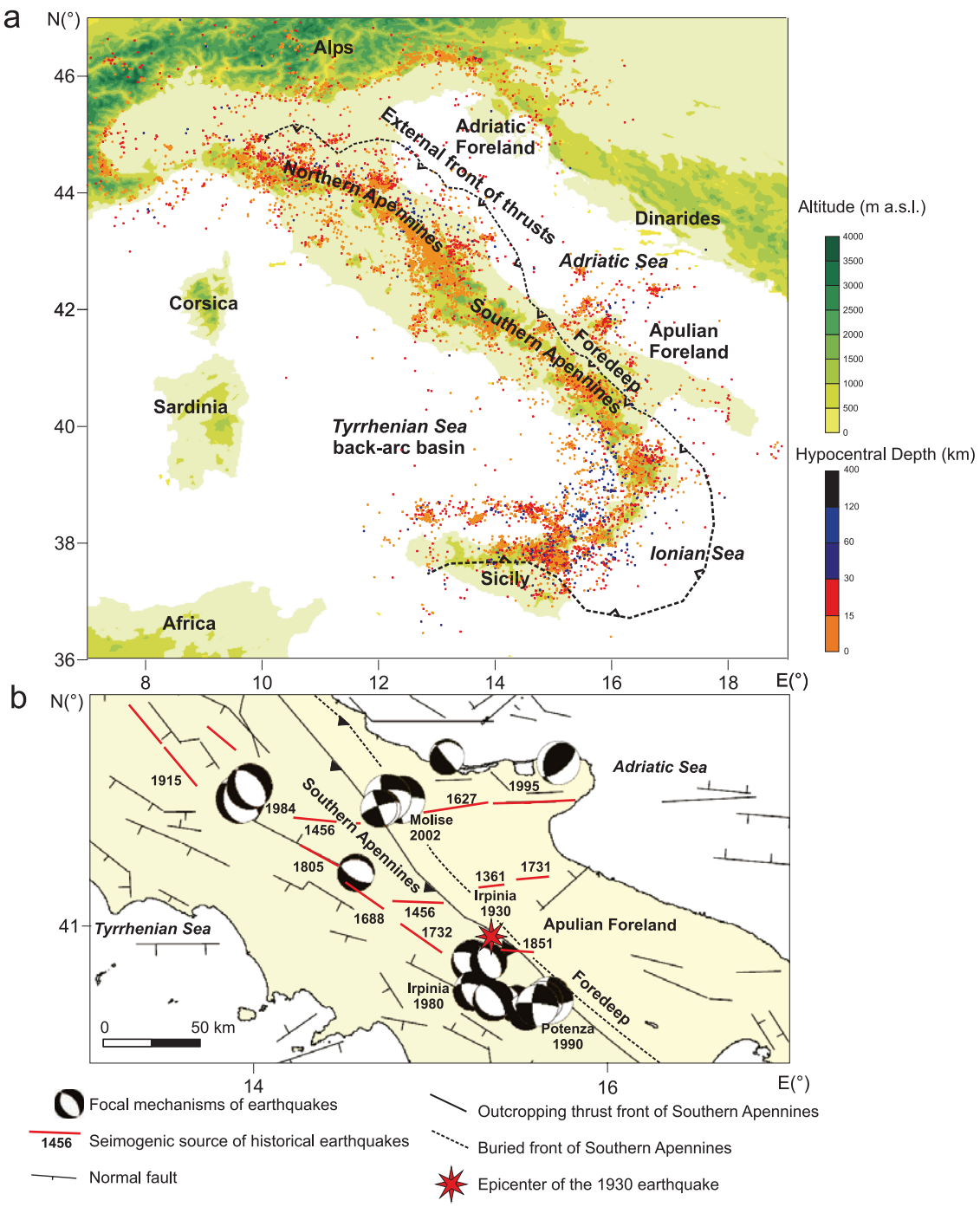

Figure 1. (a) Schematic geodynamic picture of Italy and epicentral distribution of events occurred between 1981 and 2002 (simplified and modified from *Chiarabba et al.* [2005] and *Ventura et al.* [2007]). (b) Structural map and focal mechanisms ($M_l > 3.5$) from Regional Centroid Moment Tensor catalogue http://www.ingv.it/seismoglo/RCMT/) and *Ventura et al.* [2007] (and references therein). Seismogenic sources of $M_S \geq 5.5$ historical earthquakes are from *DISS Working Group* [2006].

anomalous. For these reasons, the 1930 earthquake represents a key-event for (a) the characterization of the active tectonic processes in the peculiar subduction setting of Southern Apennines and (b) a better constrained evaluation of the seismic hazard.

[4] The scarcity of instrumental seismicity in the epicentral zone of the 1930 event prevents a precise definition of the seismotectonic picture of this area (Figure 2) and forces the analysis of the historical seismograms recorded by mechanical and early electromagnetic instruments. As demonstrated by other studies [e.g., *Kanamori*, 1988; *Pino et al.*, 2000; *Baroux et al.*, 2003; *Alvarado and Beck*, 2006], these seismograms, although hard to collect and analyze, represent an invaluable source of information for the source characterization of important past earthquakes.

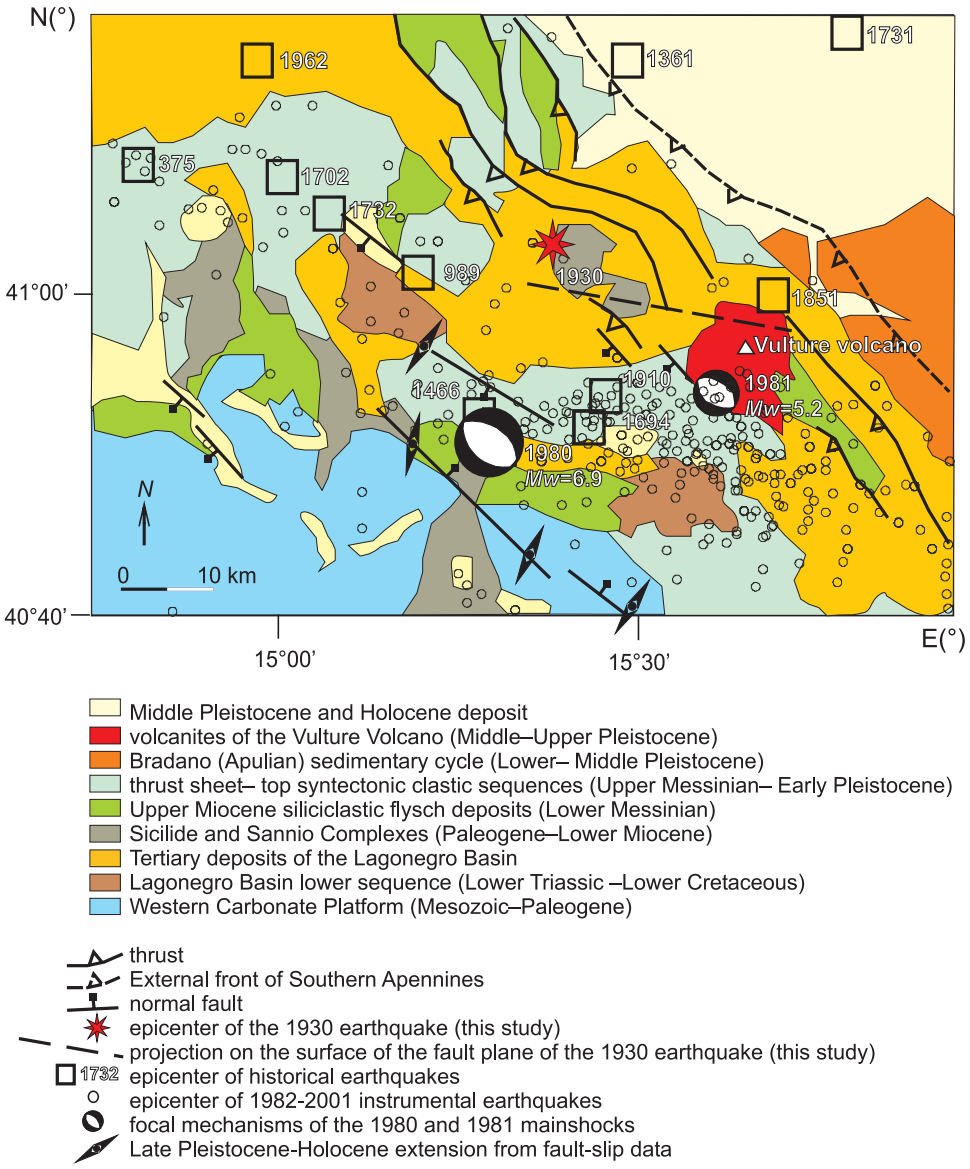

Figure 2. Geological sketch map of the Irpinia region of Southern Apennines. Geology is from *Improta et al.* [2003], epicenter and fault of the 1930 earthquake are from this study, faults and directions of extension are from *Hippolyte et al.* [1994], epicenters of historical earthquakes are from *DISS Working Group* [2006], epicenters of 1981–2002 instrumental earthquakes are from *Ventura et al.* [2007].

[5] In this paper, we study the 1930 Irpinia earthquake source by using original records from European stations. We apply modern analysis tools to obtain information on the location, magnitude, focal mechanism, seismic moment, directivity function, and slip distribution along the fault strike. We analyze the results in light of the available geological and seismological data, provide a seismotectonic picture of this area of the Apennine subduction, and discuss the geodynamic implications.

2. Geological Setting

[6] The Apennines chain is an east-verging thrust belt related to the west-dipping subduction of the Apulian lithosphere [*Doglioni et al.*, 1996, 1999]. The subduction system includes the Tyrrhenian back-arc basin to the west of the chain and the Apulia foredeep to the east (Figure 1a). The basin–thrust belt–foredeep-foreland system migrated eastward from Late Tortonian to Lower–Middle Pleistocene due to the rollback of the subducting slab [*Malinverno and Ryan*, 1986; *Patacca and Scandone*, 1989; *Patacca et al.*, 1990]. The Apennines consists of two main segments: the arc-shaped Northern Apennines and the NW-SE striking Southern Apennines, which was affected by out-of-sequence thrust-propagation processes (Figure 1a). In Lower-Middle Pleistocene, WNW-ESE striking left-lateral strike-slip faults dissected the Southern Apennines, including the Mesozoic carbonates of the western platform and the overlying accretionary wedge terrains [*Cinque et al.*, 1993; *Monaco et al.*, 2001; *Catalano et al.*, 2004]. These faults moved in response to a NE-SW compression [*Hippolyte et al.*, 1994]. From Middle-Late Pleistocene up to now, the

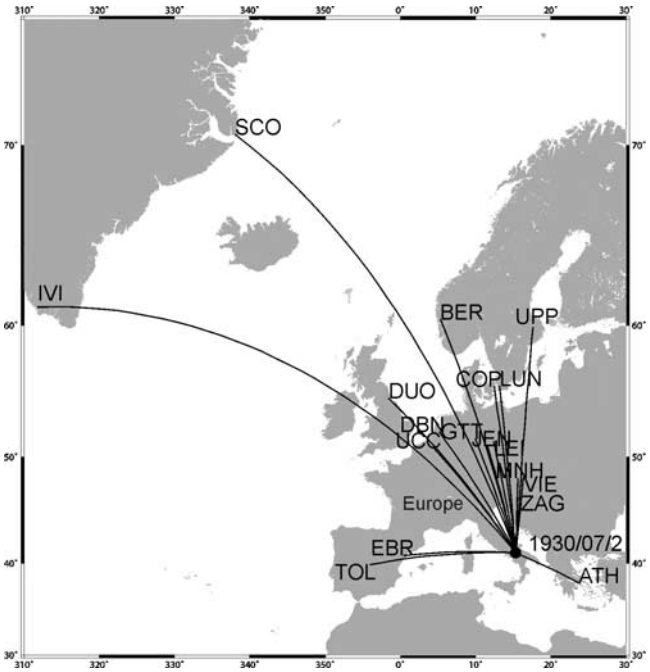

Figure 3. The great circle path to the stations where at least one seismogram was digitized and analyzed.

axial zone of Southern Apennines underwent uplift and a NE–SW extensional tectonics, which is responsible for formation of NW–SE striking faults [*Cinque et al.*, 1993; *Hippolyte et al.*, 1994]. This change in the stress regime in Pleistocene times is believed to be related to a detachment of the slab below the Southern Apennines [*Hippolyte et al.*, 1994; *Ventura et al.*, 2007]. As indicated by borehole breakouts analysis [*Amato and Montone*, 1997] and focal mechanism of large earthquakes in Southern Apennines (M_W up to 6.9) [*Chiarabba et al.*, 2005], the NE–SW extensional stress regime is still active.

[7] The Southern Apennine seismicity concentrates in the uppermost 15–20 km of the crust along the chain axis (Figure 1a) [*Chiarabba et al.*, 2005; *Ventura et al.*, 2007]. Paleoseismological, historical [*Valensise and Pantosti*, 2001b], and slip data on faults affecting Holocene terrains [*Hippolyte et al.*, 1994] confirm the above reported seismotectonic picture and reveal that the historical Apennine seismicity also concentrates along the axial zone of the chain (Figure 1b). To east, in the Apulian foreland, the seismic activity is more widespread, deeper (up to 20–30 km depth), and develops along WNW–ESE to WSW–ENE striking, right-lateral strike-slip faults. These faults are related to the larger hinge rollback rate of the Adriatic lithosphere to the north, with respect to the Apulian lithosphere to the south (Figure 1a) [*Di Luccio et al.*, 2005b; *Milano et al.*, 2005]. The seismogenic WNW–ESE striking structures which affect the easternmost sectors of the Southern Apennines chain at lat 41°.5, e.g., the fault responsible for the 1456 earthquake (Figure 1b) are interpreted as splays of the major E-W striking faults of the Apulian foreland [*Fracassi and Valensise*, 2007].

[8] The 1930 epicentral zone is located in the outer thrust system of the Southern Apennines, in an area where the deposits of the thrust sheet–top clastic sequences [Upper-Messinian–Early Pleistocene], the Miocene siliciclastic flysch, the Tertiary sequence of the Lagonegro Basin, and the vulcanites of the Vulture edifice diffusely outcrop (Figure 2). This area is one of the most active seismic zones of the Southern Apennines and large seismic events occurred in historical and more recent times: earthquakes occurred in 989, 1466, 1561, 1694, 1702, 1732, 1851, 1857, 1930, 1962, and 1980 [*Galli et al.*, 2006]. The 1466, 1694 [I_0 = X MCS], 1930 [Mw = 6.6] and 1980 [Mw = 6.9] events are the largest ones. In this area, the now inactive Apennine thrusts strike between WNW-ESE and NW-SE. The outcropping normal faults, including that responsible for the 1980 earthquake, strike NW-SE and affect the Late Pleistocene to Holocene deposits. The available gravity modeling [*Improta et al.*, 2003] of this area of Southern Apennines shows that the 1930 event epicentral zone overlies a synform-like structure characterized by an eastward thickening of the Miocene flysch deposits.

3. Waveform Data and Instrument Responses

[9] We collected seismograms from the 1930 Irpinia event in the frame of the *EuroSeismos* project [*Ferrari and Pino*, 2003]. The project itself is aimed at the digital preservation of recordings from earthquakes in the Euro-Mediterranean area and relevant station bulletins. It saw initially the participation of researchers from 15 countries, soon extended to 29 and, by the end of 2005, has been capable to put together about 25,000 historical seismograms from a list of 611 earthquakes chosen by the participants. More information can be found at http://storing.ingv.it/es_web/index.htm.

[10] For the present study we gathered 96 seismograms from 29 stations (Figure 3). Not all of the recordings are suitable for waveform digitization and analysis because of poor image quality, scarce information on the instrument response, or too slow paper speed to distinguish distinct oscillations. Sometimes the amplitude of first *P* wave arrivals is too low to be useful. Also, due to amplitude clipping, some waveforms are usable for source study from analysis of first arrivals but not for magnitude estimate. Overall, we digitized 28 seismograms from 15 stations. The epicentral distances are comprised between 4.7° and 20°, with a single station at 35°, while the azimuthal coverage is about 190°, with most stations being in 40°, between N325° and N5° (Table 1). The relative high density of stations in central/northern Europe provides redundant coverage which is particularly desirable to cross check possible errors in the data, such as wrong component polarity and instrumental constants.

[11] When possible, we recovered instrument response parameters from the original station bulletins relative to the time of the studied event, otherwise we used the instrument constants reported for closest available time period. The instrument characteristics of the stations used in the present analysis are summarized in Table 2. The set of seismometers consists of a few electromagnetic Galitzin and mostly of different types of Wiechert, very common in Europe and providing good quality recordings. In some cases, these instruments have been operating for about a century, until a

Table 1. Stations Used in the Present Study

Station	Latitude, deg	Longitude, deg	Δ, deg	Azimuth, deg	Backazimuth, deg
ATH	37.97	23.72	7.16	112.90	298.20
BER	60.38	5.33	20.31	345.57	157.71
COP	55.68	12.43	14.75	353.47	171.27
DBN	52.10	5.18	13.05	331.12	143.70
DUO	54.77	358.42	17.73	326.31	133.64
EBR	40.82	0.49	11.25	273.60	83.86
GTT	51.55	9.96	11.12	342.28	158.38
IVI	61.20	311.87	42.61	320.20	88.16
JEN	50.95	11.58	10.22	346.42	163.70
LUN	55.70	13.19	14.71	355.15	173.51
MNH	48.15	15.60	7.08	1.30	181.46
SCO	70.48	338.05	35.06	339.23	127.08
TOL	39.88	355.51	14.82	271.76	79.14
UCC	50.80	4.36	12.37	325.56	137.64
UPP	59.86	17.63	18.86	3.54	185.30
VIE	48.25	16.36	7.21	5.33	186.04
ZAG	45.83	16.00	4.78	5.32	185.75

few years ago (e.g., Uppsala, up to 1998 [*Bödvarsson*, 1999]) or are still in use (e.g., Göttingen [*Ritter*, 2002]).

4. Source Analysis

4.1. Location

[12] The ISS (International Seismological Summary) bulletin reports 112 station arrival time observations (109 *P* phase and 95 *S* phase) for the 23 July 1930 Irpinia earthquake. We used these readings and located the hypocenter of the 23 July 1930 Irpinia earthquake by means of the computer program NonLinLoc (NLL) [*Lomax*, 2005]. The code performs a probabilistic location by using an importance-sampling method based on an efficient global cascading grid-search, to obtain an estimate of the posterior probability density function (PDF) in 3D space. The cell with highest probability is divided in eight cells and this space is resampled. This procedure is repeated until a termination criterion is reached. As a result, where the probability is higher the sampling is denser. The PDF is obtained by means of an equal differential-time formulation of the likelihood function, containing the calculated and observed differences between two stations, summed over all the pairs of observations. This likelihood definition makes the algorithm independent on any origin time estimate, then the hypocenter location is reduced to a 3D problem, increasing the robustness of the method. The maximum likelihood point may be assumed as the ''optimal'' location. In case of a single, well defined, maximum, this represents a reliable estimate of the hypocenter. The procedure is applied iteratively, with automated and manual reassociation of the arrival phases and elimination of the outliers. However, due to the definition of the PDF [*Lomax*, 2005], the method is not sensitive to the presence of outliers. This feature makes NLL particularly suitable for the location of historical earthquakes, usually displaying a relatively large number of outliers, which in turn could result from phase mis-identification and difficulties in reading arrival times on analog, possibly smoked, paper recordings, and from poor clock synchronization.

[13] We used *P* and *S* waves adopting the 1D ak135 model [*Kennett et al.*, 1995] and a specific crustal model [*Basili et al.*, 1984] for traveltime computations of teleseismic and local observations, respectively. The predicted times were assigned 1 s error in order to account for 3D structural complexities. The search for the hypocentral solution was performed over the region 30°N to 50°N in latitude, 5°E to 25°E in longitude, down a depth of 700 km. We used arrival time data from the ISS bulletin and applied the procedure starting with 100 phases from 57 stations. By iteratively reassociating the phases and removing all observations with residuals greater than 3 s, the final solution (Figure 4 and Table 3) was obtained after 5 iterations, with 63 phases (38 *P* and 25 *S*) from 42 stations, with an azimuthal gap of 66°. The zone of highest PDF is well constrained in space, with a single maximum located approximately in the center. The RMS associate to this location along with the expectation hypocenter and the 68% confidence ellipsoid approximation to the PDF are also reported in Table 3. The ellipsoid represents the formal error of our hypocentral location, which gives an uncertainty of ±3.06 km in depth, ±4.9 km in the NNE direction and about ±7.7 km in the ESE direction, at an angle of 101°.

4.2. Magnitude

[14] For this earthquake, *Kárnik* [1969] obtained a magnitude M_S = 6.5, in accordance with the value $M_S = 6\frac{1}{2}$ reported by *Gutenberg and Richter* [1954]. More recently, a further instrumental estimate of M_S = 6.6 [*Margottini et al.*, 1993] and an equivalent moment magnitude M_e = 6.7 [*Gasperini et al.*, 1999] have been also published. By taking advantage of the relatively high number of seismograms collected for this study, not available before, we computed the event magnitude on each suitable waveform. The instrument parameters of Table 2 have been used to obtain the ground displacement from the original seismograms. As previously mentioned, not all the available waveforms could be used for evaluating the magnitude. On the contrary, some for which the magnitude was computed could not be used for moment rate retrieval from first *P* wave arrivals. Because of the multiple sources of error, mainly associated with uncertainties in the instrumental parameters, we preferred to compute the magnitude on each waveform, sepa-

Table 2. Characteristics of the Instruments Used in This Study[a]

		Instrument				
Station	Component	(Mechanic) (*Electromagnetic*)[a]	Mass (kg) k	Natural Period (s) T_0; T_g (s)	Magnification A_1 (mm)	Damping l (mm)
ATH	E	Wiechert	1000	7.2	165	0.404
ATH	N	Wiechert	1000	9.2	75	0.404
ATH	Z	Wiechert	1300	4.0	140	0.307
ATH	N	Mainka	136	6.0	80	0.442
BER	E	Wiechert	1000	7.5	102	0.183
BER	N	Wiechert	1000	7.5	144	0.230
COP	E	Wiechert	1000	9.6	195	0.426
COP	N	Wiechert	1000	9.6	225	0.421
COP	Z	Wiechert	1300	5.6	165	0.415
COP	N	*Galitzin*	*105*	*12.60; 12.63*	1000	125
COP	Z	*Galitzin*	95	*8.00; 11.55*	1000	*144*
COP	E	Milne-Shaw		12.0	300	0.690
COP	N	Milne-Shaw		12.0	300	0.690
DBN	E	Bosch	25	18.0	20	0.404
DBN	N	Bosch	25	18.0	20	0.404
DBN	E	*Galitzin*	*11*	*25.0; 25.0*	*1380*	*127*
DBN	Z	*Galitzin*	*175*	*12.0; 12.0*	*1380*	*6*
DUO	N	Milne-Shaw		12.0	250	0.690
EBR	E	Mainka	157	7.8	110	0.280
EBR	N	Mainka	1500	14.8	200	0.400
GTT	Z	Wiechert	1300	3.6	233	0.240
IVI	E	Wiechert	1000	9.0	210	0.404
IVI	N	Wiechert	1000	8.9	180	0.378
IVI	Z	Wiechert	1300	4.7	190	0.330
JEN	E	Wiechert	1200	9.3	240	0.311
JEN	N	Wiechert	1200	9.2	235	0.391
JEN	Z	Wiechert	1300	4.1	165	0.330
LUN	E	Wiechert	1000	11.9	197	0.515
LUN	N	Wiechert	1000	11.6	196	0.500
MNH	E	Wiechert	1200	8.9	198	0.491
MNH	N	Wiechert	1200	9.2	187	0.488
SCO	E	*Galitzin*	*39*	*9.5; 10.12*	*1000*	*12*
SCO	Z	*Galitzin*	*34*	*11.9; 11.92*	*1000*	*141*
TOL	NE	Wiechert	1000	12.5	360	0.460
TOL	NW	Wiechert	1000	12.5	250	0.460
TOL	Z	Wiechert	1200	4.5	120	0.370
UCC	E	Wiechert	1000	10.1	167	0.347
UCC	N	Wiechert	1000	10.9	145	0.367
UCC	Z	Wiechert	1300	4.8	151	0.306
UCC	E	*Galitzin*	*40*	*24.5; 24.5*	*1030*	*123.8*
UCC	N	*Galitzin*	*42*	*24.5; 24.5*	*1030*	*124.7*
UCC	Z	*Galitzin-Wilip*	*110*	*8.0; 11.5*	*106*	*6*
UPP	E	Wiechert	1000	9.1	187	0.384
UPP	N	Wiechert	1000	9.1	188	0.355
VIE	E	Wiechert	1000	11.2	210	0.400
VIE	Z	Wiechert	1200	3.0	200	0.400
ZAG	NE	Wiechert	80	5.1	15	0.520
ZAG	NW	Wiechert	80	4.3	17	0.540

[a] k is the galvanometer sensitivity factor; T_0 is the pendulum period; T_g is the galvanometer period; A_1 is the mirror-paper distance; l is the pendulum reduced length. For the Milne-Shaw only period, magnification, and damping are reported.

rately. We estimated M_S on 41 seismograms obtaining the results displayed in Table 4. Assuming the mean value as the magnitude of the 1930 event, we obtained $M_S = 6.6$.

4.3. Focal Mechanism

[15] Several authors have computed a focal mechanism for the 1930 Irpinia event (Figure 5a and Table 5). In particular, the first analysis was made by *Martini and Scarpa* [1983] who inverted 11 first motion polarities from European stations, obtaining a normal fault mechanism with about NS tensional axis. Their solution displays a considerable amount of strike slip component and nodal planes striking at N54° and N280°. Successively, *Jiménez* [1991] inverted horizontal waveforms of single station data from JEN (Germany). She tested two different crustal models in the source region, deriving different solutions: one almost pure strike slip and the other, more stable, displaying a normal fault with important strike slip component. More recently, *Emolo et al.* [2004] used 8 polarities from *Martini and Scarpa* [1983] data set and applied a couple of different methods, obtaining two solutions only differing by 10° in strike with roughly ESE–WNW striking planes. Based on forward modeling of the intensity field, they elaborate a third solution displaying same planes strike but substantially different dip, proposing the south dipping surface as the one associate to the rupture. It should be noted that the latter focal mechanism visibly does not satisfy the polarities of *Martini and Scarpa* [1983]. We integrated the first motion

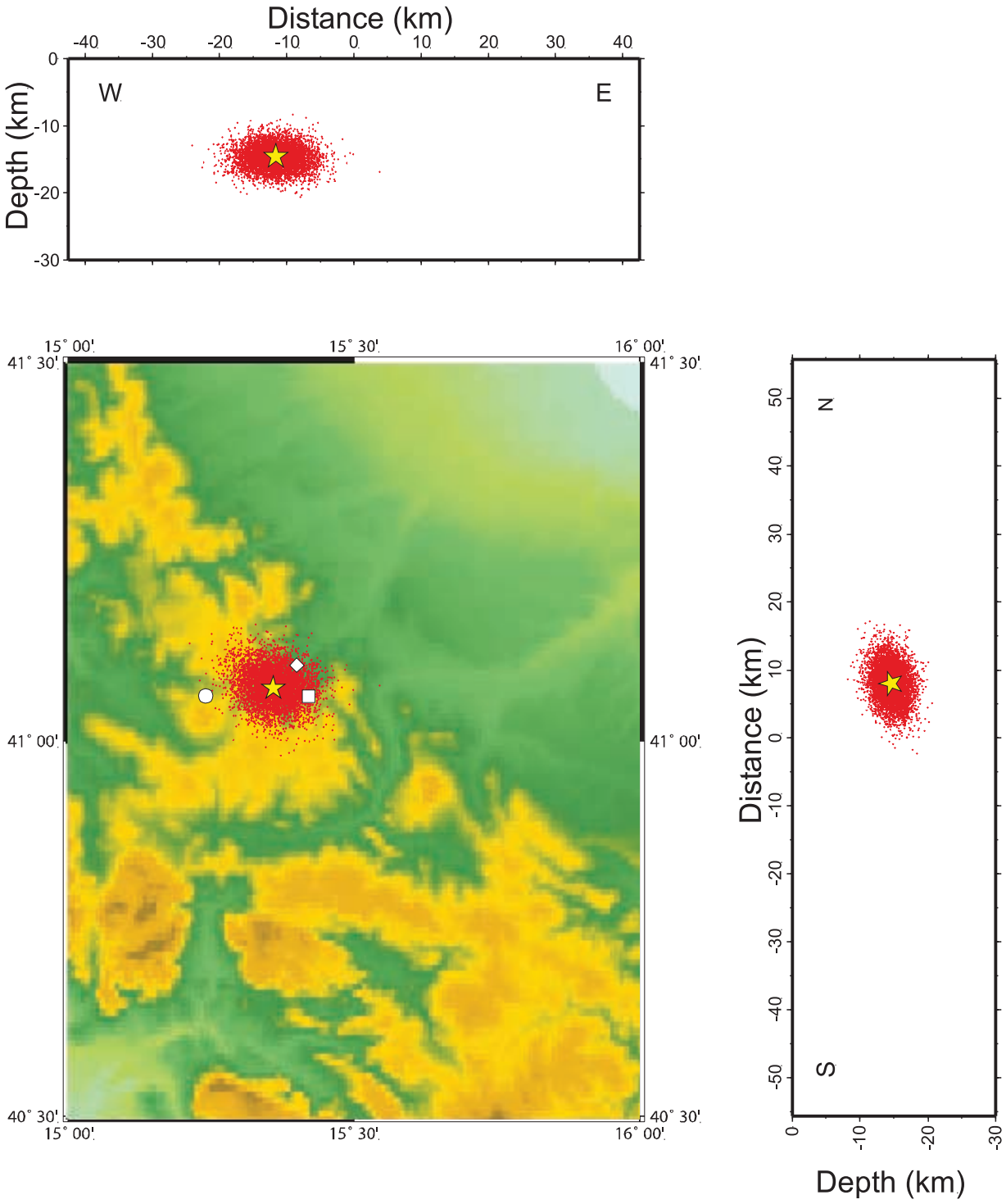

Figure 4. NonLinLoc relocation result. The PDF is represented by the clouds of red points. The yellow star indicates the maximum likelihood location. The location reported by *Oddone* [1930] (square), ISS bulletin (diamond), and *Kárnik* [1969] (circle) are also shown for comparison.

polarity data set with more readings from the collected seismograms, gathering 18 *P* wave observations in addition to 3 *SH* polarities from stations with naturally rotated components. Our best solution for the focal mechanism (Figures 5a and 5b) was obtained by using the FOCMEC package [*Snoke*, 2002]. In Figure 5b the solution is displayed along with the *P* and *SH* wave polarities.

4.4. Moment Rate Functions: Seismic Moment and Directivity Analysis

[16] We analyzed the available waveforms with the aim of getting more information about the source in terms of (1) seismic moment, (2) discrimination between the nodal planes, (3) fault extension, and (4) rupture kinematics. We attempted at the retrieval of the moment rate functions by

Table 3. HypoCentral Location of the Irpinia 1930 Event

Date	Maximum Likelihood Hypocenter					*Expect. Hypocenter*			68% Confidence Ellipsoid								
									axis 1			axis 2			axis 3		
	Time	Lat, deg	Lon, deg	Depth , km	Rms, s	*Lat, deg*	*Lon, deg*	*Depth, km*	Az, deg	Dip, deg	Len, km	Az, deg	Dip, deg	Len, km	Az, deg	Dip, deg	Len, km
07/23/1930	00:08:39.5	41.07	15.36	14.6	1.3	*41.07*	*15.36*	*14.7*	0.9	78	6.12	191	11.8	9.8	101	1	15.4

Table 4. Magnitude

Station	Component	Instrument	Magnitude
ATH	E	Wiechert	6.09
ATH	N	Wiechert	5.98
ATH	N	Mainka	6.45
ATH	Z	Wiechert	6.36
BER	E	Wiechert	7.51
BER	N	Wiechert	7.38
COP	E	Wiechert	6.53
COP	N	Wiechert	6.72
COP	Z	Wiechert	6.79
COP	N	Galitzin	6.36
COP	Z	Galitzin	6.76
COP	E	Milne-Shaw	6.3
COP	N	Milne-Shaw	6.87
DBN	E	Bosch	7.51
DBN	N	Bosch	7.09
DBN	E	Galitzin	7.21
DUO	N	Milne-Shaw	7.17
EBR	E	Mainka	6.27
EBR	N	Mainka	5.92
GTT	Z	Wiechert	6.87
IVI	E	Wiechert	6.54
IVI	N	Wiechert	6.69
IVI	Z	Wiechert	6.59
JEN	E	Wiechert	6.73
JEN	N	Wiechert	6.62
JEN	Z	Wiechert	6.75
LEI	E	Wiechert	6.63
LEI	N	Wiechert	6.2
LUN	E	Wiechert	6.48
LUN	N	Wiechert	6.62
MNH	E	Wiechert	6.38
SCO	E	Galitzin	7.1
SCO	Z	Galitzin	6.42
TOL	NE	Wiechert	6.87
TOL	NW	Wiechert	6.64
TOL	Z	Wiechert	6.16
UCC	Z	Wiechert	6.79
UCC	N	Galitzin	6.03
UPP	E	Wiechert	6.64
UPP	N	Wiechert	6.85
ZAG	NE	Wiechert	6.2

inverting *P* waveforms for the apparent source time functions (STFs). At this stage, we neglected the north component at EBR because no useful *P* pulse could be distinguished, due to the backazimuth.

[17] As previously remarked, the source geometry of the 1930 earthquake is very singular for this area and no other event recordable at regional distances has occurred in the same region area, with similar mechanism. As a consequence, no empirical Green function exists for our analysis, and then we computed synthetic seismograms. Waveforms were obtained by using a method based on the generalized ray theory [*Helmberger*, 1983] with 1-D models and the focal mechanism derived above. We also included in the computation *P* to *S* conversion at the Moho below the recording site: at regional distances this phase may have important effect, producing incorrect STF in the inversion of horizontal components when not accounted for [*Pino et al.*, 2000].

[18] The Euro-Mediterranean area is known to be characterized by strong lateral heterogeneity, in particular at upper mantle depths which affect regional recordings. Then, this approach is mostly effective when reliable structural models are known for the available source-receiver paths.

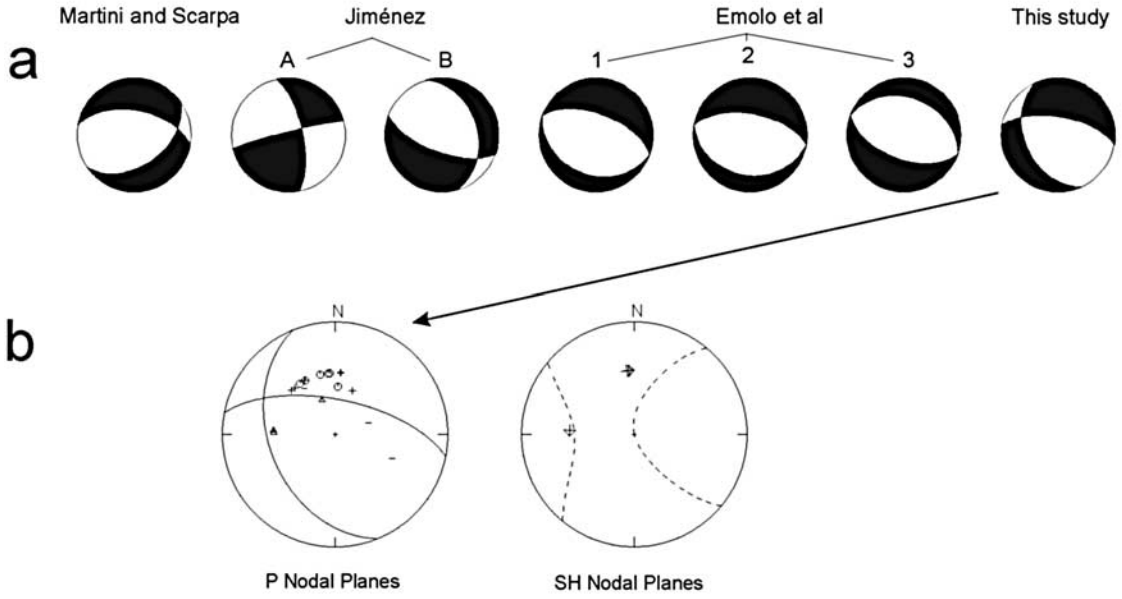

Figure 5. (a) Focal mechanism for the 1930 Irpina earthquake derived from the indicated references. The solution derived in the present study corresponds to 280, 64, −123 and 155, 41, −41, for strike, dip, and rake of the two nodal planes, respectively. (b) Focal mechanism derived in this study with indication of first motion polarities. Continuous and dashed lines represent the *P* (right) and *SH* (left) wave nodal planes, while circle and triangle mark emergent compression and dilatation, respectively.

However, *Pino et al.* [2000] demonstrated that similar STFs result when either specific or global models (e.g., PREM) are used in this region. It the same paper, by using recent events with known source characteristics, they also developed a regional model for southern Italy to-central/northern Europe paths, which proved to be very effective for STF *P* waveform inversion and here we adopted this one for the similar paths. For the western Mediterranean basin (TOL and EBR) we used the model WMP2 obtained by *Pino and Helmberger* [1997] from the waveform modeling of the upper mantle triplications. No structural model is available for the path to ATH; then, after several tests with different models resulting in no significant differences, we adopted for ATH the same model as the one used for the central European stations.

[19] We computed the moment rate function by searching for the linear combination of elementary seismograms best approximating the recorded waveforms. This is accomplished by solving the overdetermined linear system $\mathbf{Gm} = \mathbf{d}$ in the least squares sense, with the constraint of nonnegative solution. The elementary seismograms correspond to the theoretical Green function computed for 1 s triangular source and displaced by multiples of the half duration. Because of the multiple sources of error associated with the seismogram digitization and the instrumental responses, we preferred to invert separately the single waveforms. The stations azimuths with respect to the source location span more than 180° and this implies that different duration could result, whichever the real rupture plane. However, most stations are comprised in 40°, between N325° and N5°, all located in central/northern Europe. On this base, we first inverted the seismograms relative to these stations, searching for stable STFs showing significant similarities. In order to avoid the effect of the long period *PL* waves, mainly composed of crustal reverberation, we started from larger epicentral distances.

[20] The moment rate functions resulting for the waveforms from stations in central/northern Europe are displayed in Figure 6a. All the STFs have very similar shape, including the ones for the closer stations, with the stable presence of a well defined secondary maximum at the end. The durations are between 16.5 s and 20.5 s, and the seismic moment in the range 1.32×10^{18}–1.69×10^{20} Nm, with 80% comprised between 3.5×10^{18} Nm and 3.9×10^{19} Nm. In addition, we notice that the two highest values are relative to the east component of stations located approximately due north (LUN, MNH), i.e., almost transversal component; the lower signal-to-noise ratio, possible imprecise orientation of the horizontal components, and local structural heterogeneities might be affecting these results.

[21] As next step, we considered the remaining stations (TOL, EBR to the west; ATH to the east), looking for STFs with similar shape but allowing for variation in the apparent rupture time. The results are shown in Figure 6b. Different source duration is displayed at TOL, EBR, and ATH with

Table 5. Source Mechanisms for the Irpinia 1930 Event

Reference	Strike, deg	Dip, deg	Rake, deg
Martini and Scarpa [1983]	280	55	−60
Jiménez [1991] A	348	69	5
Jiménez [1991] B	343	38	−43
Emolo et al. [2004] 1	290	60	−90
Emolo et al. [2004] 2	280	60	−90
Emolo et al. [2004] 3	290	35	−90
This study	280	64	−123

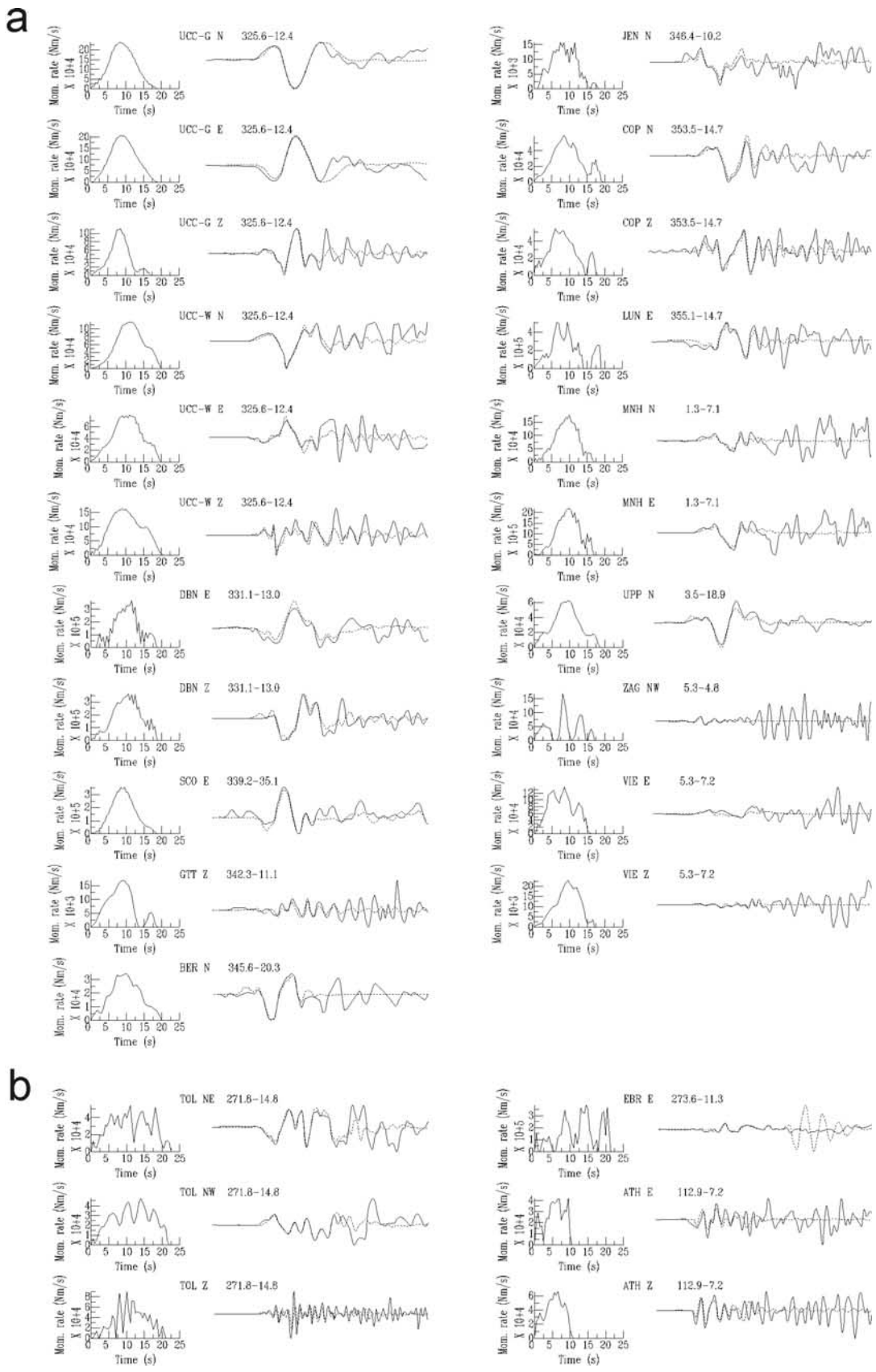

Figure 6. (a) Source time functions resulting for the 1930 Irpinia earthquake at the stations located approximately to the north, along with the comparison between data and synthetics. The numbers on top of each seismogram indicate station azimuth and distance. (b) Same as Figure 6a for the stations to the west and east.

respect to station to the north, with about 22 s to the west and 11 s to the east, with M_0 in a comparable range. The overall variability of the seismic moment for the closer stations is probably due to the structural model approximation and the effect of *PL* waves. As a matter of fact, the largest scatter results at shorter distances. In particular, M_0 relative to stations located at less than 12° are distributed in an approximately double range than the ones beyond 12°.

[22] By dropping the results for the east component of the stations located almost due north (LUN, MNH, VIE), we assumed the average value as a good estimate of the seismic moment getting 1.16 (±0.43) × 10^{19} Nm, corresponding to $M_W = 6.64$. This results is in very good agreement with the computed M_S (Table 4), but also very similar to what obtained by *Gasperini et al.* [1999] from the analysis of the felt reports.

[23] As for the apparent durations of the resulting STFs, a clear decrease from west to east is displayed. This pattern could derive from a rupture along an approximately E-W striking plane, with mostly unilateral rupture propagation toward east. If true, this would candidate the north dipping plane (strike N280°) of the focal mechanism as the one associated to the fault. We tested this hypothesis by inverting the deduced durations for fault parameters. We adopted a simple *Haskell* [1964] unilateral rupture of length L, with constant velocity v_r. Then, the apparent duration is given by:

$$t = L(1/v_r - cos\theta_r/c) \quad (1)$$

where c is the velocity of the considered waves and θ_r the station azimuth relative to the rupture direction. In principle, the rupture does not have to be parallel to the fault strike. The inversion scheme is again a least squares approach where, by keeping θ_r fixed, we searched for the best line with slope $1/L$ and intercept $-1/v_r$ approximating the data. The whole azimuth space was then spanned by 10° increments. In Figure 7a the variance is displayed as a function of the azimuth. N100°E is the angle giving the smallest value, with a very well defined minimum. This is exactly corresponding to the strike of one of the nodal planes of the focal mechanism obtained above. The best rupture length and velocity (Figure 7b) resulting for this azimuth are 32 km and 2 km/s, respectively.

[24] We also checked our results looking at the *SH* phases at EBR, where well developed *SH* components are observed. Besides, with a backazimuth of about 84°, the horizontal component at this station are almost naturally rotated. First, we derived the apparent source duration for *S* waves predicted by equation (1) for our preferred L, v_r, and fault strike; then, we computed synthetic waveforms for the stations with naturally rotated components. The comparison between predicted and recorded seismograms is shown in Figure 7c. The similarity of the waveforms corroborates the results for *P* waves obtained above, with longer apparent source duration observed to the west. In particular, the transversal component at EBR are well reproduced by the duration of 26 s predicted for a unilateral propagation of the rupture in direction approximately E–W, for a horizontal length of 32 km.

[25] In equation (1) the fracture must not necessarily propagate along the fault strike direction. In principle, L and v_r can be referred to the horizontal projection of the rupture length and velocity, respectively. On this basis, our results could be interpreted as relative to an updip break on the SW, 158°-striking plane, but this would give an unrealistic rupture length of about 42 km. We recall here that the hypocenter is at 14.6 km depth. Then, we conclude that our directivity analysis allows the discrimination of the actual fault plane, being strongly in favor of the N100E°-striking (i.e., N280°) one as responsible for the 1930 Irpinia earthquake. It is remarkable that the fault azimuth deduced from our analysis perfectly corresponds to the one obtained by *Gasperini et al.* [1999] from the analysis of the macroseismic intensity data (108° ± 11°).

[26] Following *Kanamori et al.* [1992], as successfully accomplished by *Pino et al.* [2000] for the 1908 Messina Straits earthquake, we transformed the moment rate function to obtain the slip distribution along the fault. We chose the source time function obtained for north component at COP, scaled for the evaluated seismic moment and fault length. In the hypothesis of horizontal rupture propagation and assuming a fault width of 13 km and rigidity $\mu = 3 \times 10^{10}$ N/m^2, we derived the function shown in Figure 8, where the slip value represents the width-averaged dislocation at each distance. A maximum displacement of 2 m is located approximately halfway along the strike.

[27] We also compared our results for the 1930 Irpinia event with those for the other normal fault Apenninic major earthquakes with known characteristics [*Pino et al.*, 1999; *Valensise and Pantosti*, 2001a]. In particular, the relation between seismic moment and fault length appears to be consistent, with all the events giving static stress drop ~30 bars computed for circular faults with area equivalent to a rectangular fault with aspect ratio $L/w = 2.5$.

5. Discussion and Conclusions

[28] The analysis of the original instrumental data allows us to characterize the source geometry and kinematics of the 1930 earthquake in Southern Apennines. In particular, we derive the following parameters: (1) the hypocentral location, (2) event magnitude M_S, (3) focal mechanism, (4) source time function, seismic moment, and moment magnitude M_W, (5) main source directivity, fault plane discrimination and length, and slip distribution.

[29] As reported above, we use a probabilistic approach to compute the hypocentral location. A relevant feature of our result is that, despite the presence of large outliers, the associated error is comparable to any modern event teleseismic location.

[30] The event magnitude computed on the suitable seismograms has a quite large scatter, with estimates smaller than 6 and significantly larger than 7 (Table 4). Nevertheless, the resulting average $M_S = 6.6$ is in good agreement with what computed by other authors and with the equivalent magnitude derived from intensity data [*Gasperini et al.*, 1999]. Moreover, it is almost coincident with our result for the moment magnitude ($M_W = 6.64$) obtained from the integration of the moment rate.

[31] As for the focal mechanism, except for the source A of *Jiménez* [1991], all the published solutions display normal faulting with null axis oriented approximately E-W (Figure 5a). More in detail, the sources from *Emolo et al.* [2004] are purely normal fault whereas a significant

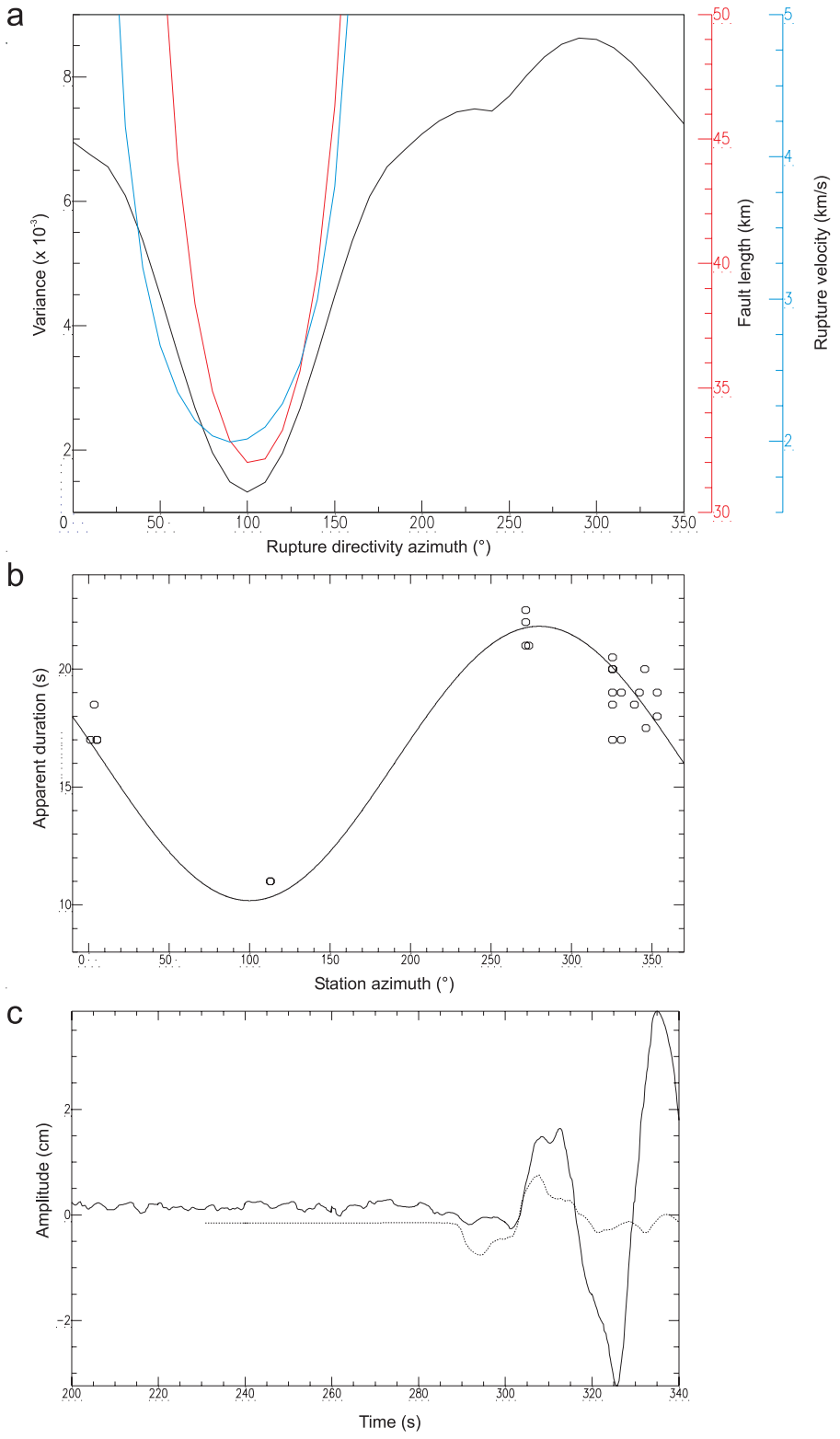

Figure 7. (a) Variance as a function of fault rupture direction (black) along with the corresponding fault length (red) and rupture velocity (blue). (b) *P* wave pulse observed duration as a function of azimuth. The curve represents the apparent duration predicted for a unilateral 32 km-long fault, propagating toward N100°E at 2 km/s. The ATH E and Z observations, at about 112°, are coincident. (c) EBR *SH* waveform compared to the synthetic computed for a source duration of 26 s. This corresponds to the apparent *S* wave duration of a 32 km-long rupture, propagating in the N100E° direction, at 2 km/s.

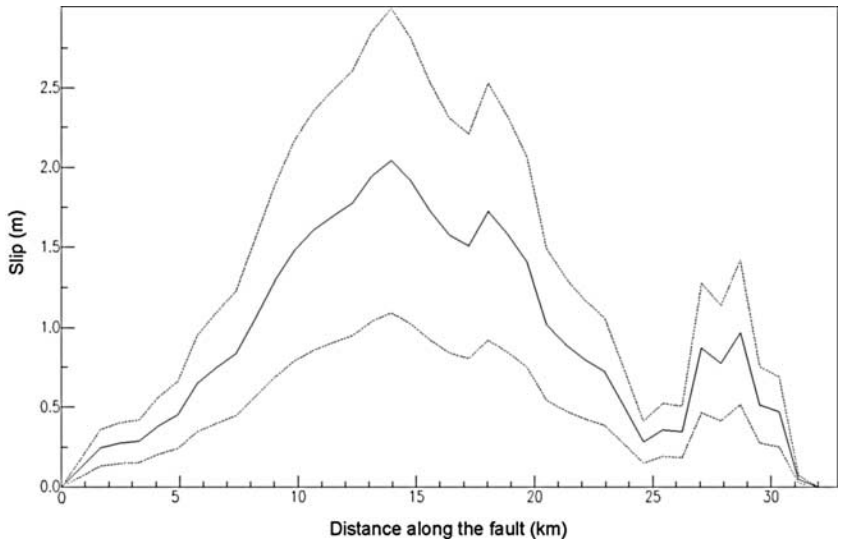

Figure 8. Along-strike slip distribution derived from the moment rate function by using a rigidity of $\mu = 3 \times 10^{10}$ N/m^2 and a fault width of 13 km. The dashed lines represent the error as derived from the seismic moment uncertainty.

strike-slip component is present by *Martini and Scarpa* [1983] and *Jiménez* [1991] B, and our solution, with the latter displaying dextral lateral component while opposite motion is associated with the others. The geodynamic interpretation of the earthquake source obviously would be different in one case or the other.

[32] Finally, the retrieved moment rate functions allowed the estimate of the rupture length and velocity, the determination of the nodal plane associated with the earthquake, and the reconstruction of the slip distribution along the fault. The estimated 32 km fault length and $M_W = 6.64$ are derived independently from each other, resulting from the duration and duration $\times$ amplitude of the source time functions, respectively. These numbers, besides being very close to what obtained from the intensity data, are in very good agreement with the empirical relation of *Wells and Coppersmith* [1994], predicting a moment magnitude of 6.66 for such a fault length. Their equations also associate a maximum displacement of 1.96 m to a normal fault with $M_W = 6.64$, very similar to our estimate of 2 m for the maximum slip.

[33] In summary, the 1930 hypocenter is located at 14.6 ± 3.06 km depth, and the focal mechanism shows an oblique (normal/right-lateral) rupture along a north dipping (64°), ESE-WNW striking plane. The rupture propagated unilaterally toward N100°E with an average velocity of 2 km/s. The average slip is 0.9 m with a maximum of 2 m at about 13 km along the fault strike and a minimum at about 25 km. A 0.8 m local slip maximum occurs at the eastern tip of the fault (Figure 8).

[34] The above results are crucial in the individuation of the fault responsible of this important event in Southern Apennines, the interpretation of its geodynamic significance, and the evaluation of the associated hazard. The rupture of the 1930 event nucleated within the southwest dipping carbonate rocks of the Apulian platform, which extends from 10 to 18 km depth (Figures 9a and 9b). Our results indicate that the eastern tip of the 1930 fault crosses the Vulture volcano (Figure 2), whose last activity (132 ka) produced multiple WNW–ESE aligned monogenic cones [*De Astis et al.*, 2006]. An explanation for the 0.8 m local slip maximum may be the propagation of the rupture trough the high rigidity, completely crystallized Vulture plumbing system.

[35] The hypocentral depth of the 1930 event is consistent with that of the major seismic events of Southern Apennines (e.g., the 1980, Mw = 6.9 event; depth = 12 km; [*Bernard and Zollo*, 1989; *Chiarabba et al.*, 2005]). These latter earthquakes affected the flysch units and carbonates of the chain and were characterized by almost purely normal slips along NW–SE striking faults moving in response to a NE–SW extension [*Frepoli and Amato*, 2000; *Ventura et al.*, 2007]. On the contrary, the 1930 hypocenter is within the Mesozoic carbonates of the Apulian foredeep-foreland (Figures 9a and 9b), and its focal mechanism displays oblique slip (normal-right-lateral) along a N280° striking fault moving in response to the same extension direction. Therefore the kinematics of the 1930 event significantly differs from that typical of Southern Apennines earthquakes and late Pleistocene to Holocene outcropping faults [*Hippolyte et al.*, 1994; *Galli et al.*, 2006]. In fact, the 1930 fault strike is nearly the same of the E-W dextral strike-slip faults responsible for the 1851 (I_0 = X MCS), 1990, M_{Wmax} = 5.8, Potenza sequence, and 2002, M_{Wmax} = 5.8, Molise seismic sequences [*Di Luccio et al.*, 2005a, 2005b]. Both the 1990 and 2002 main shocks nucleated within the Apulian domain, in response to the stress field acting within the foreland, which is characterized by a NW–SE compression and NE–SW extension [*Milano et al.*, 2005]. However, while the 2002 epicenters locate in the foreland, east of the thrust front, the 1851, 1990 and 1930 epicenters locate immediately west of the Southern Apennines thrust front and east of the chain axis (Figure 9a). The two 1456 earthquakes (I_0 = X MCS), occurred along north dipping, N280° striking fault segments at about 25 and 75 km, respectively, northwest of the 1930 event, also locate

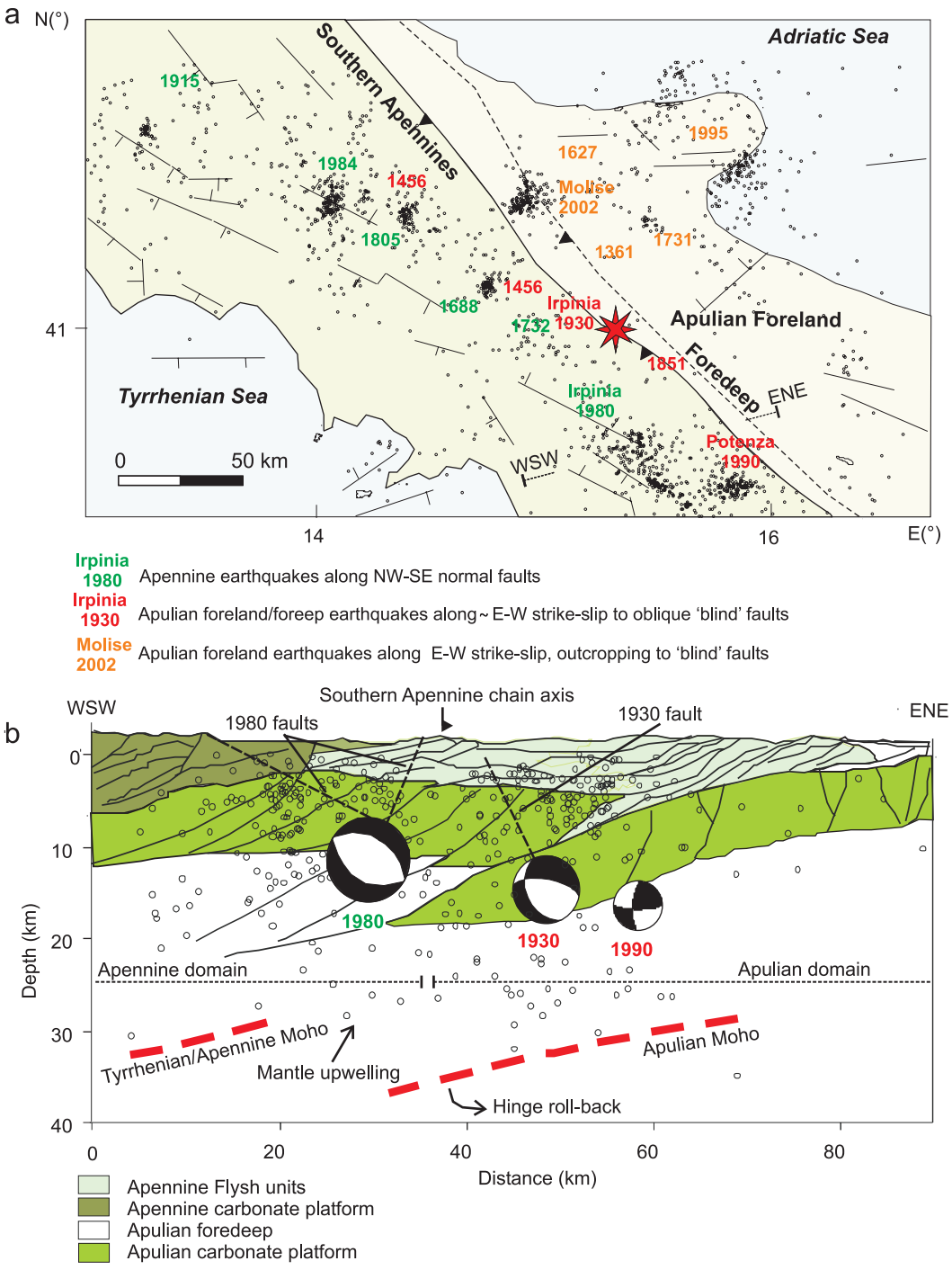

Figure 9. (a) Interpretative sketch of the Southern Apennine seismotectonic setting (data from Figure 1b). (b) Depth distribution of the seismicity in Southern Apennines on interpreted seismic reflection profile (modified from *Ventura et al.* [2007]). Events fall within a ± 30 km band. Focal mechanisms of the 1980 and 1990 events are from *Di Luccio et al.* [2005b]. Focal mechanism of the 1930 earthquake is from this study (Figure 5b). The trace of the faults of the 1930 earthquake (this study) and 1980 events [*Amoruso et al.*, 2005] are also reported. The main geodynamic processes are summarized according to *Doglioni et al.* [1996, 1999] and *Ventura et al.* [2007].

between the chain axis and the thrust front [*Fracassi and Valensise*, 2007]. Therefore the 1930 earthquake occurred in the same structural domain of the 1851, 1990, and 1456 earthquakes, i.e., in the zone of transition between the chain, which is characterized by NW–SE striking normal faults related to the upwelling of the mantle wedge beneath Southern Apennines [*Ventura et al.*, 2007], and the foreland, which, according to [*Doglioni et al.*, 1996, 1999] is affected by strike-slip to oblique, E–W to WNW–ESE striking faults moving in response to the higher hinge rollback of

the Adriatic lithosphere with respect to the Apulian lithosphere (Figure 9b). The seismic belt depicted by the 1456, 1851, 1930, and 1990 earthquakes is within this back-rolling, hinge zone of the Apulian lithosphere, which is characterized by WNW–ESE to E–W striking faults that date back to the Mesozoic age [*Chilovi et al.*, 2000]. We propose that the above reported events developed along these faults, which, on the basis of the 1930 and 1990 focal mechanisms, move with oblique or strike-slip kinematics depending on depth and locally prevailing Apennines or foreland stress fields. Finally, it is worth nothing that surface failure is not reported for any of these earthquakes, suggesting that the seismogenic faults underlying the external sector of Southern Apennines mainly affect the Apulian carbonates. This observation rules out the possibility that the 1456, 1930, and 1990 events represent the re-activation of the outcropping WNW–ESE striking strike-slip faults that dissected the flysch and underlying carbonates of the Southern Apennines chain in Lower-Middle Pleistocene [*Catalano et al.*, 2004] (see also section 2). We conclude that the sector of the Apulian foreland-foredeep underlying the Southern Apennines chain is affected by WNW–ESE "blind" faults capable of highly destructive events like the 1930 earthquake. Geophysical and geochemical investigations are needed to detect the possible occurrence of other seismogenic "blind" structures.

[36] **Acknowledgments.** We thank R. Console, R. Scarpa, and J. Batlló for comments and suggestions, L. Arcoraci for help with seismograms digitations, and C. Piromallo, L. Improta, F.R. Cinti, U. Fracassi, R. Di Giovambattista, and G. Milano for the numerous discussions on the geodynamic significance of the Southern Apennine seismicity. This work is supported by INGV funds.

References

Alvarado, P., and S. Beck (2006), Source characterization of the San Juan (Argentina) crustal earthquakes of 15 January 1944 (Mw 7.0) and 11 June 1952 (Mw 6.8), *Earth Planet. Sci. Lett.*, doi:10.1016/j.epsl.2006.01.015.

Amato, A., and P. Montone (1997), Present day stress field and active tectonics in southern peninsular Italy, *Geophys. J. Int.*, *130*, 519–534.

Amoruso, A., L. Crescentini, and R. Scarpa (2005), Faulting geometry for the complex 1980 Campania-Lucania earthquake from levelling data, *Geoph. J. Int.*, *162*, 156–168, doi:10.1111/j.1365-246X.2005.02652.x.

Baroux, E., N. A. Pino, G. Valensise, O. Scotti, and M. E. Cushing (2003), Source parameters of the 11 June 1909, Lambesc (Provence, southeastern France) earthquake: A reappraisal based on macroseismic, seismological, and geodetic observations, *J. Geophys. Res.*, *108*(B9), 2454, doi:10.1029/2002JB002348.

Basili, A., G. Smriglio, and G. Valensise (1984), Procedure di determinazione ipocentrale in uso presso l'Istituto Nazione di Geofisica, *Atti III Convegno G.N.G.T.S.*, Roma, 875–884.

Bernard, P., and A. Zollo (1989), The Irpinia (Italy) 1980 earthquake: Detailed analysis of a complex normal faulting, *J. Geophys. Res.*, *94*(B2), 1631–1647.

Bödvarsson, R. (1999), The new Swedish seismic network, *ORFEUS Newslett.*, *l*(3), 22.

Catalano, S., C. Monaco, L. Tortorici, W. Paltrinieri, and N. Steel (2004), Neogene-quaternary tectonic evolution of the southern Apennines, *Tectonics*, *23*, TC2003, doi:10.1029/2003TC001512.

Chiarabba, C., L. Jovane, and R. Di Stefano (2005), A new view of Italian seismicity using 20 years of instrumental recordings, *Tectonophysics*, *395*, 251–268, doi:1016/j.tecto.2004.09.013.

Chilovi, C., A. J. De Feyter, and A. Pompucci (2000), Wrench zone reactivation in the Adriatic Block: The example of the Mattinata fault system (SE Italy), *Boll. Soc. Geol. It.*, *119*, 3–8.

Cinque, A., E. Patacca, P. Scandone, and M. Tozzi (1993), Quaternary kinematic evolution of the Southern Apennines. Relationship between surface geological features and deep lithospheric structures, *Ann. Geophys.*, *36*, 249–260.

De Astis, G., P. D. Kempton, A. Peccerillo, and T. W. Wu (2006), Trace element and isotopic variations from Mt. Vulture to Campanian volcanoes: Constraints for slab detachment and mantle inflow beneath southern Italy, *Contrib. Mineral. Petrol.*, *151*, 331–351, doi:10.1007/s00410-006-0062-y.

Di Luccio, F., E. Fukuyama, and N. A. Pino (2005a), The 2002 Molise earthquake sequence: What can we learn about the tectonics of Southern Italy?, *Tectonophysics*, *405*, 141–154, doi:10.1016/j.tecto2005.05.024.

Di Luccio, F., A. Piscini, N. A. Pino, and G. Ventura (2005b), Reactivation of deep faults beneath Southern Apennines: Evidence from the 1990–1991 Potenza seismic sequences, *Terra Nova*, *17*, 586–590, doi:10.1111/j.1365-3121.2005.00653.x.

DISS Working Group (2006), Database of Individual Seismogenic Sources (DISS), Version 3.0.2: A compilation of potential sources for earthquakes larger than M 5.5 in Italy and surrounding areas. http://www.ingv.it/DISS/

Doglioni, C., P. Harabaglia, G. Martinelli, F. Mongelli, and G. Zito (1996), A geodynamic model of the southern Apennines, *Terra Nova*, *8*, 540–547.

Doglioni, C., E. Gueguen, P. Harabaglia, and F. Mongelli (1999), On the origin of W-directed subduction zones and applications to the western Mediterranean, *Geol. Soc. Am. Spec. Pap.*, *156*, 541–561.

Emolo, A., G. Iannaccone, A. Zollo, and A. Gorini (2004), Inferences on the source mechanisms of the 1930 Irpinia (southern Italy) earthquake from simulations of the kinematic rupture process, *Ann. Geophys.*, *47*, 1743–1754.

Ferrari, G., and N. A. Pino (2003), Euroseismos 2002-2003, a project for saving and studying historical seismograms in the Euro-Mediterranean area, *Geophys. Res. Abstr.*, *5*, 05274.

Fracassi, U., and G. Valensise (2007), Unveiling the sources of the catastrophic 1456 multiple earthquake: Hints to an unexplored tectonic mechanism in southern Italy, *Bull. Seismol. Soc. Am.*, *97*, 725–748, doi:10.1785/0120050250.

Frepoli, A., and A. Amato (2000), Stress tensor orientation in peninsular Italy from background seismicity, *Tectonophysics*, *317*, 109–124.

Galli, V. Bosi, S. Piscitelli, A. Giocoli, and V. Scionti (2006), Late Holocene earthquakes in southern Apennine, paleoseismology of the Caggiano fault, *Int. J. Earth. Sci.*, *95*, 855–870, doi:10.1007/s00531-005-0066-2.

Gasperini, P., F. Bernardini, G. Valensise, and E. Boschi (1999), Defining seismogenic sources from historical felt reports, *Bull. Seismol. Soc. Am.*, *78*, 94–110.

Gutenberg, B., and C. F. Richter (1954), *Seismicity of the Earth and Associated Phenomena*, 2nd ed., Princeton University Press, Princeton, New Jersey.

Haskell, N. A. (1964), Total energy and energy spectral density of elastic wave radiation from propagating faults, *Bull. Seismol. Soc. Am.*, *54*, 1811–1842.

Helmberger, D. V. (1983), Theory and application of synthetics seismograms, in *Earthquakes: Observation, Theory and Interpretation, Proc. Int. Sch. Phys. Enrico Fermi, Course LXXXV*, edited by H. Kanamori and E. Boschi, pp. 174–222, North-Holland, Amsterdam.

Hippolyte, J. C., J. Angelier, and F. Roure (1994), A major geodynamic change revealed by Quaternary stress patterns in the Southern Apennines (Italy), *Tectonophysics*, *230*, 199–210.

Improta, L., M. Bonagura, P. Capuano, and G. Iannaccone (2003), An integrated geophysical investigation of the upper crust in the epicentral area of the 1980, Ms = 6.9, Irpinia earthquake (Southern Italy), *Tectonophysics*, *361*, 139–169, doi:10.1016/S0040-1951(02)00588-7.

Jenny, S., S. Goes, D. Giardini, and H. G. Kahle (2006), Seismic potential of Southern Italy, *Tectonophysics*, *415*, 81–101, doi:10.1016/jtecto.2005.12.003.

Jiménez, E. (1991), Focal mechanism of some European earthquakes from the analysis of single station long-periods record, in *Seismicity, Seismotectonics and Seismic Risk of the Ibero-Maghrebian Region*, edited by J. Mezcua and A. Udias, pp. 87–96, Monografia N° 8, IGN, Madrid.

Kanamori, H. (1988), Importance of historical seismograms for geophysical research, in *Historical Seismograms and Earthquakes of the World*, edited by W. H. K. Lee et al., pp. 16–33, Academic Press, San Diego.

Kanamori, H., H.-K. Thio, D. Dreger, E. Hauksson, and T. Heaton (1992), Initial inverstigation of the Landers, California earthquake of 28 June 1992 using TERRAscope, *Geophys. Res. Lett.*, *19*(22), 2267–2270.

Kárnik, V. (1969), *Seismicity of the European Area, Part 1, D*, Reidel Publishing Company, Doordrecht, Holland.

Kennett, B. L. N, E. R. Engdahl, and R. Buland (1995), Constraints on seismic velocities in the Earth from travel times, *Geophys. J. Int.*, *122*, 108–124.

Lomax, A. (2005), A reanalysis of the hypocentral location and related observations for the great 1906 California earthquake, *Bull. Seismol. Soc. Am.*, *95*, 861–877, doi:10.1785/0120040141.

Malinverno, A., and B. F. Ryan (1986), Extension in the Tyrrhenian Sea and shortening in the Apennines as result of arc migration driven by sinking of the lithosphere, *Tectonics*, *5*(2), 227–245.

Margottini, N. N. Ambraseys, and A. Screpanti (1993), La magnitudo dei terremoti italiani del XX secolo, *Internal Publication, E.N.E.A.*, Rome, Italy.

Martini, M., and R. Scarpa (1983), Earthquake in the Italy in last century, in *Earthquakes: Observation, Theory and Interpretation, Proc. Int. Sch. Phys. Enrico Fermi, Course LXXXV*, edited by H. Kanamori and E. Boschi, pp. 479–492, North-Holland, Amsterdam.

Milano, G., R. Di Giovambattista, and G. Ventura (2005), Seismic constraints on the present-day kinematics of the Gargano foreland, Italy, at the transition zone between the southern and northern Apennine belts, *Geophys. Res. Lett.*, *32*, L24308, doi:10.1029/2005GL024604.

Monaco, C., L. Tortorici, S. Catalano, W. Paltrinieri, and N. Steel (2001), The role of Pleistocene strike-slip tectonics in the Neogene-Quaternary evolution of the Southern Apennine orogenic belt: Implications for oil trap development, *J. Petrol. Geol.*, *24*, 339–359.

Oddone, E. (1930), Studio sul terremoto avvenuto il 23 luglio 1930 nell'Irpinia, Relazione a il Ministro dell'Agricoltura e Foreste, S.E., *13*. *La Meteorologia Pratica*, *Regio Ufficio Centrale di Meteorologia e Geofisica*.

Patacca, E., and P. Scandone (1989), Post-Tortonian mountain building in the Apennines. The role of the passive sinking of a relic lithospheric slab, in *The Lithosphere in Italy, Advances in Earth Science Research, Atti dei Convegni Lincei*, vol. 80, edited by A. Boriani et al., pp. 157–176, Accademia Nazionale dei Lincei, Roma.

Patacca, E., R. Sartori, and P. Scandone (1990), Tyrrhenian Basin and Apenninic arcs: Kinematic relations since Late Tortonian times, *Mem. Soc. Geol. It.*, *45*, 425–451.

Pino, N. A., and D. V. Helmberger (1997), Upper mantle compressional velocity model beneath the western Mediterranean basin, *J. Geophys. Res.*, *102*(B2), 2953–2967.

Pino, N. A., S. Mazza, and E. Boschi (1999), Rupture directivity of the major shocks in the 1997 Umbria-Marche (central Italy) sequence from regional broadband waveforms, *Geophys. Res. Lett.*, *26*(14), 2101–2104.

Pino, N. A., D. Giardini, and E. Boschi (2000), The December 28, 1908, Messina Straits, southern Italy, earthquake: Waveform modeling of regional seismograms, *J. Geophys. Res.*, *105*(B11), 25,473–25,492.

Ritter, J. R. R. (2002), On the recording characteristics of the original Wiechert seismographs at Göttingen (Germany), *J. Seismol.*, *6*, 477–486.

Snoke, J. A. (2002), FOCMEC: FOcal MEChanism determinations, in *International Handbook of Earthquake and Engineering Seismology, Part B*, edited by W. H. K. Lee et al., chap. 85.12, pp. 1629–1630, Academic Press, San Diego.

Valensise, G., and D. Pantosti (2001a), Database of potential sources for earthquakes of magnitude larger than M 5.5 in Italy, *Ann. Geophys.*, *44*, suppl. 4, 175.

Valensise, G., and D. Pantosti (2001b), The investigation of potential earthquake sources in peninsular Italy: A review, *J. Seismol.*, *5*, 287–306.

Ventura, G., F. R. Cinti, F. Di Luccio, and N. A. Pino (2007), Mantle wedge dynamics versus crustal seismicity in the Apennines (Italy), *Geochem. Geophys. Geosyst.*, *8*, Q02013, doi:10.1029/2006GC001421.

Wells, D. L., and K. J. Coppersmith (1994), New empirical relationships among magnitude, rupture length, rupture width, rupture area, and surface displacement, *Bull. Seismol. Soc. Am.*, *84*, 974–1002.

G. Ferrari, SGA srl, Via del Battiferro 10/b, 40129 Bologna, Italy.

B. Palombo, Istituto Nazionale di Geofisica e Vulcanologia, Centro Nazionale Terremoti, Via di Vigna Murata 605, 00143 Rome, Italy.

B. Perniola, Istituto di Fisica, Università degli Studi di Urbino, Via S. Chiara, 27, 61029 Urbino, Italy.

N. A. Pino, Istituto Nazionale di Geofisica e Vulcanologia, Osservatorio Vesuviano, Via Diocleziano 328, 80124 Naples, Italy. (napino@ov.ingv.it)

G. Ventura, Istituto Nazionale di Geofisica e Vulcanologia, Sismologia e Tettonofisica, Via di Vigna Murata 605, 00143 Rome, Italy.